Sensors & Diagnostics

PAPER

View Article Online
View Journal | View Issue

Cite this: *Sens. Diagn.*, 2024, **3**, 431

MXene quantum dots for ratiometric fluorescence detection of a *Bacillus anthracis* biomarker

Chunxiao Lin, Chubei Qiu, Yanan Wang, Yaowen Liu, Mingcong Rong * and Li Niu

As a new member of the quantum dot (QD) family, MXene QDs (MQDs) have attracted increasing attention in fluorescence sensing because of their excellent photostability and resistance to photobleaching. MQD-based fluorescent sensors are still at the initial stage, especially ratiometric fluorescence methods with higher accuracy and sensitivity. Herein, blue fluorescent MQDs are prepared by acid oxidation and hydrothermal methods using Ti_3C_2 MXene as the precursor. The MQDs are rich in hydroxyl and amino groups, which can coordinate with EDTA and Eu^{3+} to form the composite probe MQDs–EDTA–Eu^{3+}. The MQDs–EDTA–Eu^{3+} complex emits the blue fluorescence of MQDs since Eu^{3+} is surrounded by H_2O molecules, which are excellent quenchers to the fluorescence of Eu^{3+}. 2,6-Dipicolinic acid (DPA) is a biomarker of *Bacillus anthracis*, and also an excellent ligand of Eu^{3+}. With the addition of DPA, it can replace the H_2O molecule to form the MQDs–EDTA–Eu^{3+}–DPA complex, stimulating the intense red fluorescence of Eu^{3+} at 616 nm due to the absorbance energy-transfer effect (AETE) from DPA to Eu^{3+}. In the meantime, the fluorescence of MQDs at 445 nm remains stable as a reference signal. In consequence, the MQDs–EDTA–Eu^{3+} complex is used to construct a ratiometric fluorescence method for DPA detection for the first time, with a linear detection range of 0–11 μM and a detection limit of 0.26 nM. Furthermore, an MQD-based test paper is fabricated for the visual detection of DPA, with a low detection limit of 52.4 nM. This work indicates that MQDs have potential applications in the area of visual fluorescence sensing.

Received 26th November 2023,
Accepted 17th January 2024

DOI: 10.1039/d3sd00314k

rsc.li/sensors

1. Introduction

Bacillus anthracis is a Gram-positive bacterium that poses a serious threat to living organisms and is considered a biological warfare agent. Inhalation of 10^4 anthrax spores will induce death if the patient does not receive timely treatment within 48 hours. Therefore, rapid, sensitive, and selective detecting techniques for anthrax spores are essential to prevent outbreaks of anthrax disease and biochemical attacks.[1–3] 2,6-Dipicolinic acid (DPA) is the major component of anthrax spores, accounting for about 5–15% of the dry weight of *Bacillus anthracis*, and is recognized as a biomarker for bacillus spores.[4] Therefore, the detection of DPA becomes important for realizing the monitoring of *Bacillus anthracis*.[1,3] To date, various DPA detection methods have been developed, such as surface-enhanced Raman spectrometry,[5] electrochemiluminescence,[6] and colorimetry.[7] Though they have achieved some good results, they suffer drawbacks such as expensive instruments, long reaction time, tedious sample pretreatment, and complex operation, which seriously limit their development. Therefore, an analytical method with simple operation, fast reaction speed, economic cost, high sensitivity, and good selectivity is urgently needed to be developed for DPA detection.

Fluorescence analysis technology has received tremendous attention in disease diagnosis, food inspection, and environmental monitoring due to the merits of high sensitivity, high reproducibility, simplicity and easy integration.[8,9] A large number of fluorescent probes have been reported for DPA detection, such as lanthanide ion-based metal–organic frameworks,[1,10] boron carbon oxynitride quantum dots,[11] carbon dots,[12] covalent organic frameworks,[13] SiO_2 nanoparticles,[14] europium–organic gels nanosheets,[15] and so on. Recently, ratiometric fluorescence methods relying on a reference signal and a response signal have been popular due to their self-calibration, higher accuracy, higher precision, and visualization effect.[16,17] Particularly, the ratiometric fluorescence method of a probe was combined with Eu^{3+} for DPA detection.[1,18] Additionally, intense red fluorescence of Eu^{3+} can be activated through the coordination of DPA to Eu^{3+}. Coupling with blue or green fluorescent probes, an obvious color variation can be observed by the naked eye.[11,20] However, the visualization by eye can only realize qualitative detection and semi-

Guangzhou Key Laboratory of Sensing Materials and Devices/Center for Advanced Analytical Science/School of Chemistry and Chemical Engineering, Guangzhou University, Guangzhou 510006, China. E-mail: rongmc@gzhu.edu.cn

quantitative detection. A smartphone with a camera and color recognition software can easily and quickly achieve quantitative detection, and has become a hot topic recently.[21]

MXenes are a kind of promising two-dimensional nanomaterial, and were discovered by Prof. Gogotsi and his team through selectively etching MAX. In the MAX structure, M represents an early transition metal, A represents aluminum or silicon, and X is carbon or nitrogen.[22] Owing to their large surface area, wide absorption range, superior conductivity, and favorable hydrophilicity,[23,24] MXenes are widely used in energy storage,[25] biomedicine,[26] and sensing.[27] MQDs prepared by acid oxidation and hydrothermal synthesis not only inherit the advantages of their precursor MXenes, including the relatively high surface area, and wide absorption range, but also the properties of QDs, such as the excellent dispersion, sensitive terminating groups, and excellent optical properties.[28] Thus, MQDs are one of the potential probes for fluorescent sensors.[9] For example, amino-functionalized MQDs were used to diagnose histidine in human serum through the inner filter effect (IFE),[28] MQDs were used to detect uric acid through a fluorescence resonance energy transfer effect[29] and N-doped MQDs were also used to detect H_2O_2 and xanthine through the photoinduced electron-transfer (PET) effect.[30] All the above reports indicate that fluorescent MQDs can serve as fluorescence probes. However, most MQD-based fluorescent sensors have a single emission response,[31–35] and ratiometric fluorescence methods are still rare.[29,30,36–40] Furthermore, no MQDs have been reported to be used for DPA or *Bacillus anthracis* detection.

In this work, blue fluorescent MQDs were prepared through acid oxidation and hydrothermal processes. The optimal excitation and emission wavelengths were 265 nm and 445 nm. The fluorescent composite probe MQDs–EDTA–Eu^{3+} was self-assembled by the coordination of MQDs, EDTA, and Eu^{3+}. After the addition of DPA, it can stimulate the intense red fluorescence of Eu^{3+} at 616 nm through the AETE effect by the Eu^{3+}–DPA complex. In the meantime, the fluorescence of MQDs at 445 nm serves as an internal reference. Consequently, a ratiometric fluorescent sensor for the detection of DPA was constructed for the first time. This work also indicates the promising application of MQDs in fluorescence sensing.

2. Experimental section

2.1 Materials and chemicals

Ti_3AlC_2, hydrofluoric acid (HF, 40%), diammonium phosphate (DAP), urea, ethylene diamine tetraacetic acid (EDTA), and europium nitrate hexahydrate ($Eu(NO_3)_3{\cdot}6H_2O$) were purchased from Aladin Ltd. Dipicolinic acid (DPA), phthalate (PH), picolinic acid (PA), nicotinic acid (NA), and isonicotinic acid (ISA) were purchased from Sigma-Aldrich, Inc. Benzoic acid (BA), 36.0–38.0% hydrochloric acid (HCl) and 65.0–68.0% nitric acid (HNO_3) were purchased from Guangzhou Chemical Reagent Factory (China). L-Cysteine (Cys), L-leucine (Leu), L-arginine (Arg), and phenylalanine (Phe) were purchased from Macklin Biochemical Co., Ltd (China). All unlabeled concentrations of chemicals used in the experiments are analytical grade. Ultrapure water with a resistivity of 18.25 MΩ cm^{-1} was used in the whole experiment.

2.2 Synthesis of Ti_3C_2 MXene

Ti_3C_2 MXene was obtained using the HF acid etching method: 1 g Ti_3AlC_2 was slowly added into 10 mL 40% HF acid, and the mixture solution was stirred for 12 hours at room temperature. Then, the reacted solution was diluted into 50 mL ultrapure water. The Ti_3C_2 MXene solution was centrifuged (5000 rpm, 5 min) and washed with ultrapure water several times until the pH was close to 7. Finally, the Ti_3C_2 MXene was collected by vacuum filtration, and the Ti_3C_2 MXene powder was obtained by freeze-drying.

2.3 Synthesis of MQDs

First, 300 mg Ti_3C_2 MXene was added to an oil bath of 12 mL concentrated hydrochloric acid and 4 mL nitric acid for 5 hours at 100 °C to obtain Ti_3C_2 MXene with a few layers. After cooling to room temperature, the reaction solution was poured into a beaker containing a 100 mL ice–water mixture, and the pH value was adjusted to 7 by adding NaOH.[19]

Then the hydrothermal method was used to prepare MQDs. The above reaction solution and 0.6 g DAP were added into a Teflon-lined autoclave chamber and heated at 120 °C for 12 h. After the solution cooled down, the supernatant solution was transferred into a 1000 Da dialysis bag with ultrapure water for 24 hours.[19] The final MQD solution was stored in a refrigerator at 4 °C for the subsequent experiments.

2.4 Ratiometric fluorescence detection of DPA

50 μL EDTA (2 mM) and 50 μL $Eu(NO_3)_3$ (2 mM) were added into a centrifuge tube containing 50 μL MQD solution. Then, PBS buffer (10 mM, pH: 7.0) solution containing different concentrations (0, 0.001, 0.005, 0.01, 0.025, 0.05, 0.075, 0.1, 0.15, 0.2, 0.25, 0.5, 1, 3, 5, 7, 9, 11 μM) of DPA was added. The final volume of the solution was 1 mL. The fluorescence spectra were collected 5 min after the solution was prepared. In the selective detection, the concentration of the interfering substance and DPA was 11 μM. The excitation wavelength was set as 265 nm and a long pass filter (380 nm) was used to eliminate interference from the excitation light.

2.5 The visual detection of DPA

First, a circular hole punch was used to make the paper substrate. Commercial filter paper was cut into circular paper with a diameter of *ca.* 6 mm. Then, 20 μL MQDs–EDTA–Eu^{3+}

probe solution containing 1 mM EDTA, 1 mM Eu^{3+}, and MQDs was added onto the circular paper and dried naturally at room temperature. The MQD-based test papers were obtained.

10 μL DPA solution of different concentrations (1–200 μM) was dropped onto the MQD-based test paper, and photos of these test papers were taken under a 254 nm ultraviolet lamp using a smartphone. The RGB values of the fluorescence photos were extracted by color recognition software. Then the DPA concentration standard curve was drawn according to the ratio of the R/B value.

2.6 Determination of DPA in real water samples

Real water samples were taken from the Pearl River, Guanggong River, Zhishan Lake, and tap water. Real water samples were purified by centrifuging (10 000 rpm, 5 min) and filtering with a 0.22 μm membrane. 20 μL water sample was added into the solution containing the probe solution and different concentrations of DPA (0, 5, 7, 9 μM). The DPA concentration was obtained by plugging the value of F_{616}/F_{445} into the standard working curve.

3. Results and discussion

3.1 Morphology and structure characterization of MQDs

As shown in Scheme 1, multi-layer Ti_3C_2 MXene was first prepared by etching the inner Al atomic layer of the Ti_3AlC_2 MAX phase with concentrated hydrofluoric acid. A scanning electron microscope (SEM) was used to investigate the morphology of Ti_3C_2 MXene. As shown in Fig. 1a, Ti_3C_2 MXene presents a multi-layered, accordion-like structure. Then, strong acid oxidation was conducted to cut multi-layer Ti_3C_2 MXene into small pieces (Fig. 1b). Finally, MQDs were synthesized by hydrothermal cutting of Ti_3C_2 MXene with the pore-forming reagent DAP. Transmission electron microscopy (TEM) was used to investigate the morphology of MQDs. As shown in Fig. 1c, the synthesized MQDs are monodispersed spherical particles, with a mean diameter of 4.22 nm and a lattice spacing of 0.272 nm (Fig. 1d and e), corresponding to the Ti_3C_2 MXene (010).[41] The result also indicated that the MQDs kept the structure characteristic of MXene.

To investigate the structure of Ti_3C_2 MXene, X-ray diffraction (XRD) measurement was conducted. As shown in Fig. 2a, the raw material Ti_3AlC_2 MAX corresponded well to the standard card (No. 52-0875). Likewise, for Ti_3C_2 MXene, the characteristic (002) peak shifted slightly to the left (from 9.5° to 8.9°), indicating that the as-prepared Ti_3C_2 MXene kept the main crystal structure characteristics of Ti_3AlC_2 MAX.[42] The disappearance of the peak at 39° [Al(104)] implied that the Al atomic layer was etched away.[28] For MQDs, a broadened and blue-shifted peak before 10° could be observed, indicating that the crystallinity of MQDs was lower than MXene.[43] The Fourier transform infrared (FT-IR) spectra were also obtained to study the functional groups of MXene and MQDs. As shown in Fig. 2b, the absorption band around 3407 cm^{-1} corresponded to the O–H bond, and both MXene and MQDs contained abundant O–H groups.[33,44] After the acid oxidation and hydrothermal process, MQDs possess abundant hydrophilic functional groups, resulting in their favorable water solubility.[31] Two new stretching vibration peaks at 2031 cm^{-1} and 1374 cm^{-1} corresponded to the N–H bond and the O–H bond.[36] The MQDs possess much more O–H groups than that of the MXene after undergoing the acid oxidation process, and the surface potential of MQDs is negative (Fig. 2c). Another two absorption bands at 1078 cm^{-1} and 1633 cm^{-1} were assigned to the stretching vibrations of C–O and C=O bonds. The peaks at 756 cm^{-1}

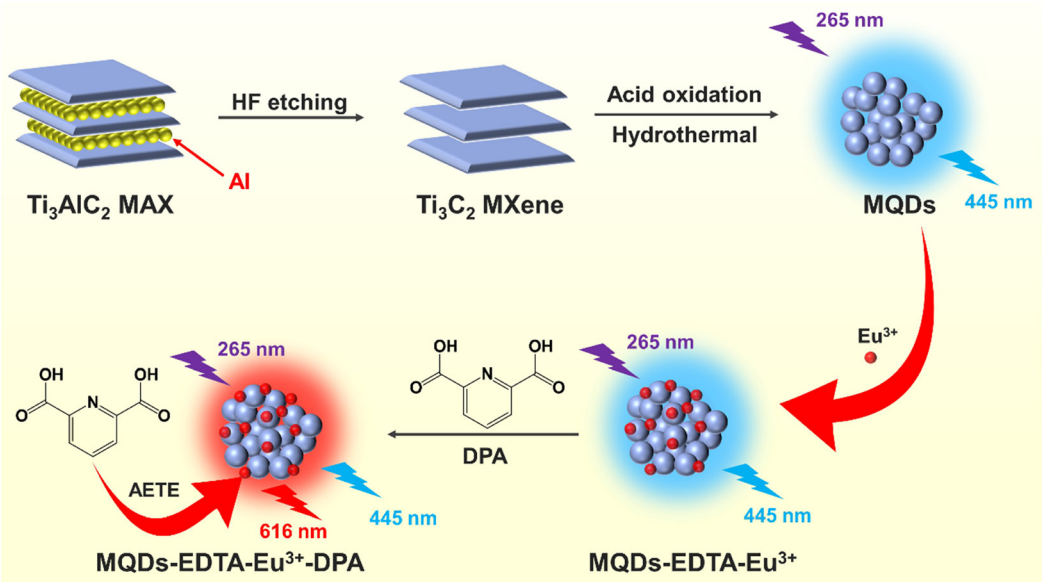

Scheme 1 The preparation of MQDs and fluorescent MQDs–EDTA–Eu^{3+} complex for DPA sensing.

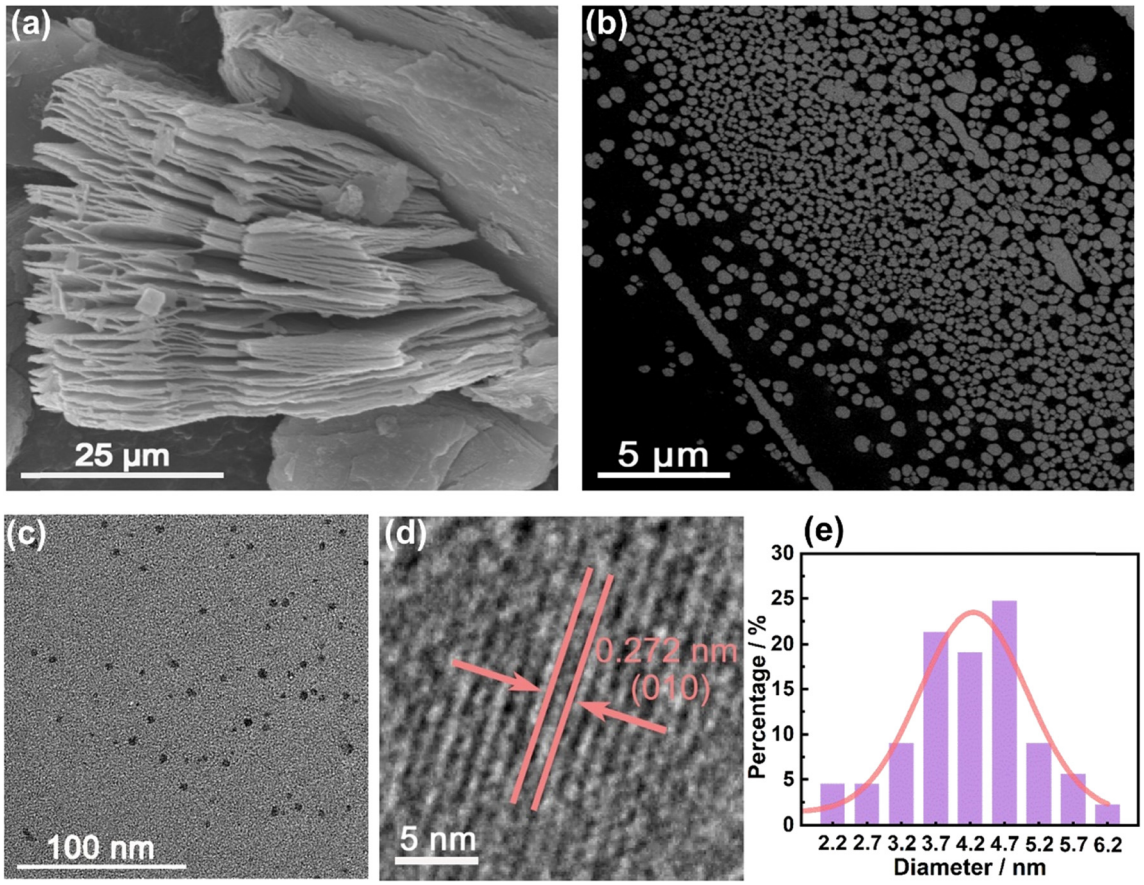

Fig. 1 (a) SEM image of Ti_3C_2 MXene. (b) SEM image of Ti_3C_2 MXene after acid oxidation. (c) TEM image, (d) HRTEM image, and (e) the corresponding size distribution of MQDs.

and 539 cm^{-1} corresponded to the vibration of the Ti–O bond and Ti–C bond.[29,33]

X-ray photoelectron spectroscopy (XPS) was conducted to further study the functional groups and surface composition of MQDs. As shown in Fig. 2d, there were five peaks at 133.5, 284.8, 400.0, 455.2, and 532.3 eV in the XPS spectrum of MQDs, which are attributed to P 2p (6.70%), C 1s (50.27%), N 1s (3.56%), Ti 2p (0.16%), and O 1s (39.31%), respectively. The three peaks of C 1s at 284.8, 286.3, and 288.4 eV corresponded to the C–C, C–O/C–N, and C═O/C═N bond, respectively (Fig. 2e).[31] The three peaks of O 1s at 531.1, 532.4, and 535.8 eV were assigned to the C–O, C═O, and N–O bond, respectively (Fig. 2f).[41,45] The three peaks of N 1s at 398.8, 399.8, and 401.4 eV were ascribed to the C–N–C, N–$(C)_3$ and N–H, respectively (Fig. 2g).[46] The two peaks of P 2p at 133.3 and 134.3 eV were attributed to P–O and P–C/P–N, respectively (Fig. 2h).[47] The four peaks of Ti 2p corresponded to Ti–O (458.2 and 464.0 eV) and Ti–C (458.8 and 464.8 eV), respectively (Fig. 2i).[48] The functional groups verified by XPS spectra are consistent with that of the FT-IR spectra results.

3.2 The fluorescence sensing of DPA

The optical properties of MQDs were investigated by UV-vis absorption and fluorescence spectroscopy. As shown in Fig. 3a, MQDs have a broad absorption band from 250 to 325 nm, which corresponds to the trapping of the excited state energy by the surface states.[49] The optimum fluorescence excitation and emission spectra of MQDs were 265 nm and 445 nm, respectively, and the optimal excitation and emission were consistent with the three-dimensional fluorescence spectra as shown in Fig. 3b. The solution of MQDs was clear and transparent for about six months (Fig. 3a inset picture), which proves that MQDs have excellent water solubility and dispersibility. The photoluminescence quantum yield (PLQY) of the MQDs was determined to be 0.97%. Though the PLQY of MQDs is relatively low, the MQDs showed excellent anti-photobleaching properties (Fig. 3c), and their fluorescence intensity remains at 93% after 1 h UV irradiation at 265 nm. Meanwhile, the fluorescence intensity of MQDs remains stable for about one month, indicating that MQDs are a kind of potential probe for fluorescence sensing.

The fluorescence excitation wavelength just overlaps with the maximum fluorescence excitation of Eu^{3+} (270 nm)[11] and there is a wide range (~171 nm) between the fluorescence emission between MQDs and Eu^{3+}, which indicates that there is a possibility to fabricate a visual fluorescent sensor towards DPA by the MQDs–EDTA–Eu^{3+} probe. The zeta potential results also confirmed their self-

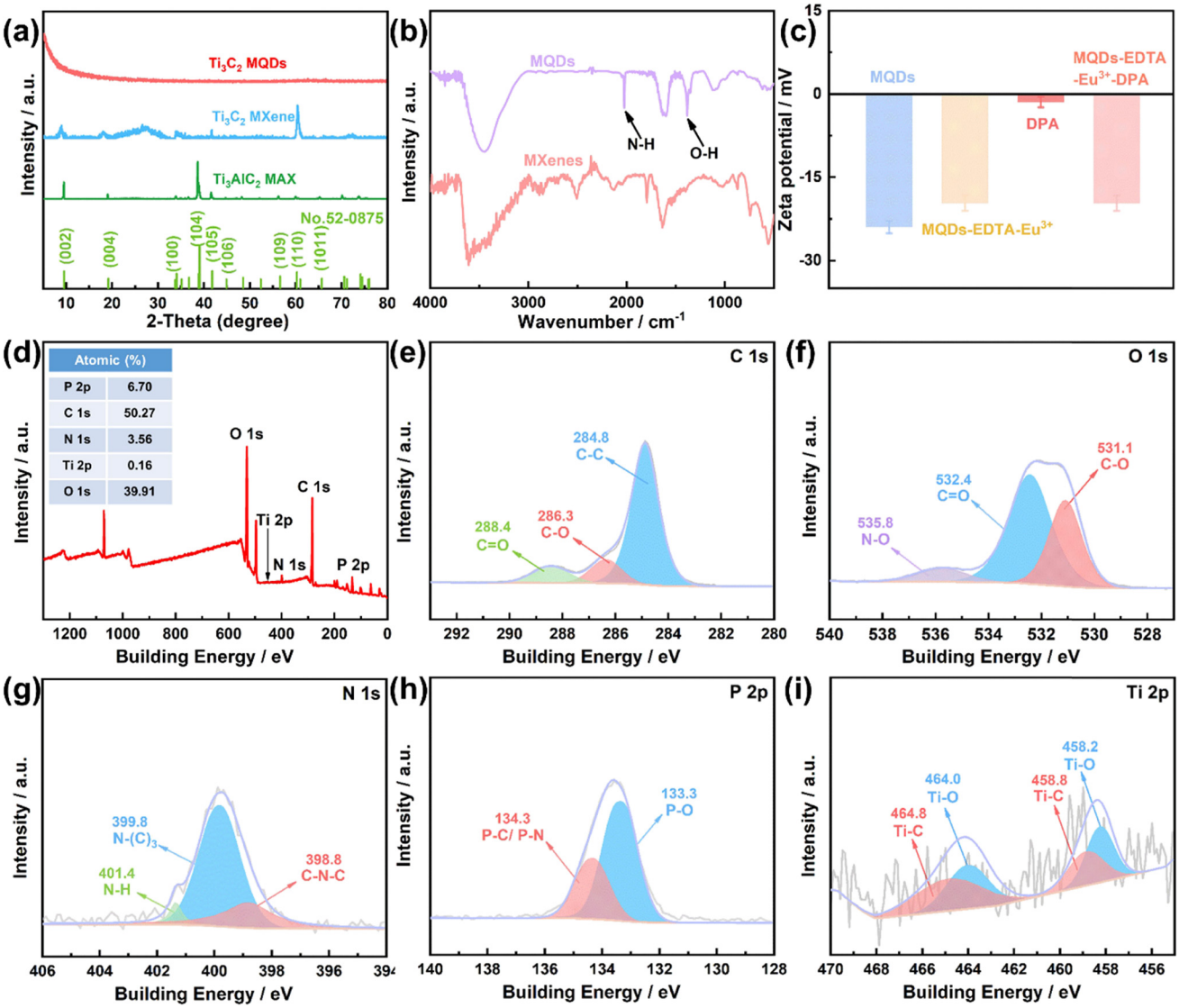

Fig. 2 (a) XRD patterns of Ti_3AlC_2 MAX, Ti_3C_2 MXene and MQDs. (b) FT-IR spectra of Ti_3C_2 MXene, and MQDs. (c) Zeta potential of MQDs, MQDs–EDTA–Eu^{3+}, DPA, and MQDs–EDTA–Eu^{3+}–DPA. (d) XPS spectra and high-resolution XPS spectra of (e) C 1s, (f) O 1s, (g) N 1s, (h) P 2p, and (i) Ti 2p for MQDs.

assembly possibility. The surface potential of MQDs is −24.0 mV (Fig. 2c) while that of MQDs–EDTA–Eu^{3+} increases to −19.7 mV due to electrostatic interaction between MQDs and EDTA–Eu^{3+}. After the addition of DPA (−1.4 mV), the surface potential of MQDs–EDTA–Eu^{3+}–DPA decreased to −22.7 mV. This suggested that DPA could interact with MQDs–EDTA–Eu^{3+}. The results are consistent with previous reports.[50]

The ratiometric fluorescence detection method is generally composed of a constant reference signal and a sensitive response signal.[12,51] Recently, the ratiometric fluorescence detection method has been popular for its accurate and sensitive results owing to its background-free and self-calibrating merits.[51,52] To achieve a better sensitivity, pH and incubation time were tested. As shown in Fig. 3e, the fluorescence intensity of the MQDs remained stable in the pH range from 3 to 11, and the quenching efficiency became stable in the pH range from 7 to 11. The fluorescence intensity at 445 and 616 nm became constant within 5 min (Fig. 3f). In consequence, the following experiments were conducted at pH 7.0 for 5 min.

As shown in Fig. 3g, the fluorescent probe MQDs–EDTA–Eu^{3+} emits the same blue fluorescence at 445 nm as MQDs under an excitation wavelength of 265 nm. The fluorescence of Eu^{3+} is quenched by the coordinated water molecules.[11] After the addition of DPA, water molecules were substituted by DPA, accompanied by the intense fluorescence of Eu^{3+}.[53] DPA is an efficient antenna molecule (the absorption peak of DPA is 272 nm)[11] which can absorb the excitation light at 265 nm and then transfer the absorbed energy to Eu^{3+}, stimulating the red

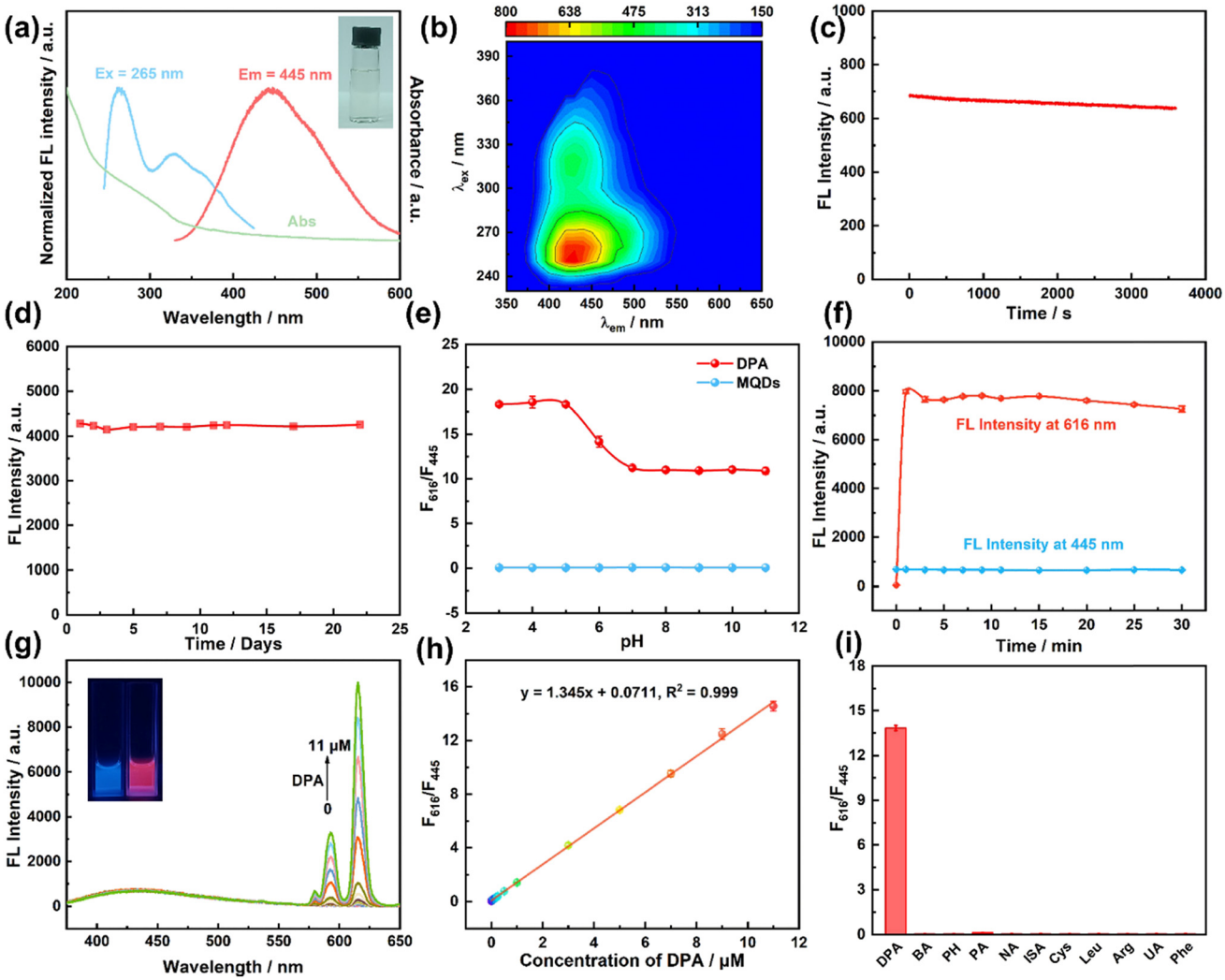

Fig. 3 (a) UV-vis absorption spectrum, fluorescence excitation, and emission spectra of MQDs (inset: the photograph of the MQD solution in natural light). (b) The three-dimensional fluorescence spectrum of MQDs. (c) The photostability of MQDs. (d) The photostability of MQDs for about one month. Effects of (e) pH and (f) incubation time (blue line: fluorescence intensity of MQDs at 445 nm; red line: fluorescence intensity of Eu^{3+} at 616 nm) on the detection sensitivity of the sensor. (g) Fluorescence spectra and (h) corresponding fluorescence intensity standard curve of F_{616}/F_{445} towards different concentrations of DPA. (i) Fluorescence responses of the MQDs–EDTA–Eu^{3+} complex to various interferents.

fluorescence emission of Eu^{3+} at 593 nm and 616 nm. In the meantime, the blue fluorescence of MQDs at 445 nm remains constant. As a consequence, a ratiometric fluorescence detection method for DPA was developed according to the fluorescence intensity ratio of $F_{616/445}$ and DPA concentration. As shown in Fig. 3g, with the addition of DPA, the fluorescence intensity at 616 nm gradually increased while the fluorescence intensity at 445 nm remained stable. Meanwhile, the fluorescence of the reaction solution changed from blue to red after DPA was added (the inset photo in Fig. 3g). A linear relationship of F_{616}/F_{445} = 1.35[DPA] + 0.0711 ranging from 0 to11 μM was obtained, with a correlation coefficient of 0.999 and a limit of detection (LOD) of 0.26 nM (according to the signal-to-noise ratio of 3) (Fig. 3h). This method also exhibited excellent selectivity; none of other interfering substances disturbed the detection results (Fig. 3i).

3.3 Visual detection of DPA by the MQD-based test paper

To date, fabrication point-of-care testing techniques using visual test strips combined with a smartphone have attracted extensive attention.[54–57] Herein, a portable and simple MQD-based test paper was prepared for the visual detection of DPA. As shown in Fig. 4, the fluorescence color of the MQD-based test paper gradually varied from blue to red as the concentration of DPA increased from 0 to 200 μM under a 254 nm UV lamp. The fluorescence photos were captured by the camera in the smartphone, and the photo color information (R/B ratio values) was analyzed by a color recognition app, which was used as a quantitative determination parameter for DPA detection.[11,58] A linear relationship of R/B = 0.00906[DPA] + 0.238 (R^2 = 0.999) with a very low LOD of 52.4 nM was found. The MQD-based test paper for DPA detection implies the potential practicability of

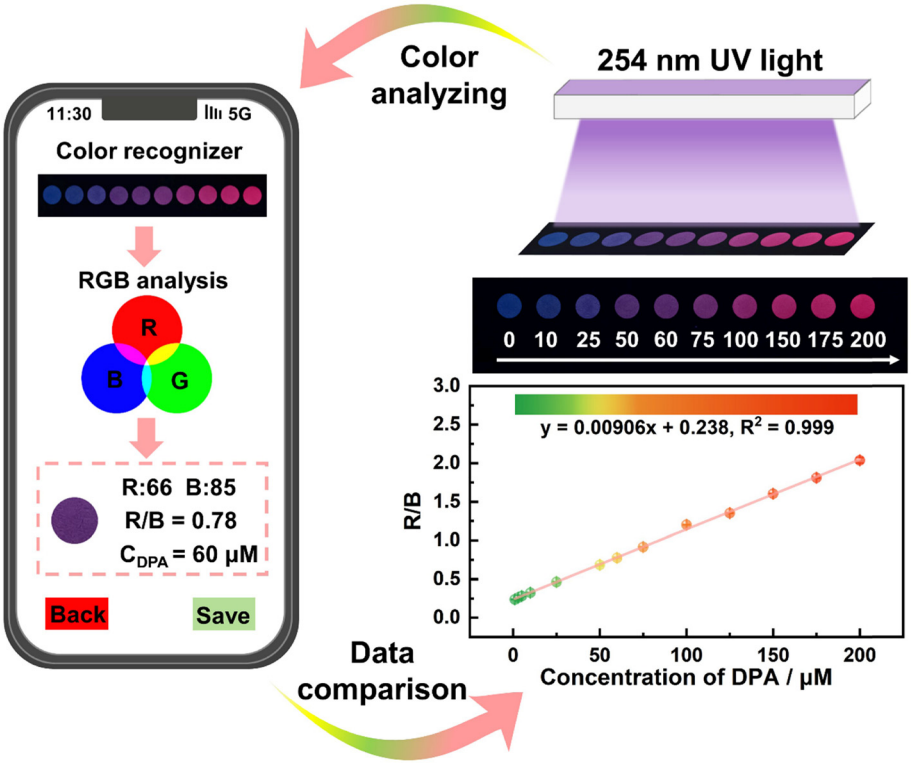

Fig. 4 The MQD-based test paper for the visual detection of DPA under a 254 nm UV lamp.

MQD-based test paper for fluorescence sensing applications in the future.

3.4 Real water sample analysis

To evaluate the practical application of this method, the MQD-based fluorescent sensor was applied for DPA determination in real water samples. Tap water, Zhishan Lake water, Guanggong Lake water, and the Pearl River water were selected. As shown in Table 1, the recoveries of the water samples varied in the range of 81.00–112.44%, and the relative standard deviation (RSD) was still less than 0.32%. These results indicated that the proposed method showed potential practical application.

Table 1 Fluorescence detection of DPA in spiked real water samples (n = 3)

Samples	Added (μM)	Found (μM)	Recovery (%)	RSD (%)
Tap water	0	Not found	—	—
	5	4.14	82.80	0.20
	7	6.68	95.43	0.19
	9	9.63	107.00	0.12
Zhishan Lake	0	Not found	—	—
	5	4.65	93.00	0.29
	7	6.25	89.29	0.27
	9	8.92	99.11	0.32
Guanggong River	0	Not found	—	—
	5	4.89	97.80	0.19
	7	7.40	105.71	0.28
	9	10.12	112.44	0.19
The Pearl River	0	Not found	—	—
	5	4.05	81.00	0.16
	7	6.15	87.86	0.04
	9	8.35	92.78	0.11

4. Conclusion

In summary, blue fluorescent MQDs were prepared by the facile acid oxidation and hydrothermal method. The MQDs show favorable water solubility and photostability. Based on the AETE effect, MQDs were successfully used to build a ratiometric fluorescent sensor for DPA detection, with a linear range of 0–11 μM and a LOD of 0.26 nM. Furthermore, MQD-based test paper was developed for the visual detection of DPA, with a low LOD of 52.4 nM. This work broadens the ratiometric fluorescence sensing application of MQDs. Furthermore, MQDs for the first time served as a novel nanomaterial for the rapid and sensitive detection of anthrax biomarkers.

Author contributions

Chunxiao Lin: methodology, investigation, validation, and writing – original draft. Chubei Qiu: investigation. Yanan Wang: software. Yaowen Liu: data curation. Mingcong Rong: conceptualization, funding acquisition, and writing – review & editing. Li Niu: supervision and funding acquisition.

Conflicts of interest

The authors declare that they have no known competing financial interests or personal relationships that could have appeared to influence the work reported in this paper.

Acknowledgements

This work is supported by the National Youth Foundation of China (21904027), the Natural Science Foundation of Guangdong Province (2019A1515011328), the Science and Technology Projects in Guangzhou (202201000002), and the Key Discipline of Materials Science and Engineering, Bureau of Education of Guangzhou (202255464).

References

1 L. Yu, L. Feng, L. Xiong, S. Li, S. Wang, Z. Wei and Y. Xiao, *J. Hazard. Mater.*, 2022, **434**, 128914.
2 P. P. Zhang, A. Y. Ni, J. J. Zhang, B. L. Zhang, H. A. Zhou, H. Zhao, S. Liu, J. Ni and C. Duan, *Sens. Actuators, B*, 2023, **384**, 133624.
3 L. Han, X. Z. Dong, S. G. Liu, X. H. Wang, Y. Ling, N. B. Li and H. Q. Luo, *Environ. Sci.: Nano*, 2023, **10**, 683–693.
4 X. Niu, M. Wang, M. Zhang, R. Cao, Z. Liu, F. Hao, L. Sheng and H. Xu, *Inorg. Chem. Front.*, 2022, **9**, 4582–4593.
5 Y. Yao, J. Ji, H. Zhang, K. Zhang, B. Liu and P. Yang, *Anal. Chem.*, 2018, **90**, 10394–10399.
6 S. Y. Xiao, S. J. Zhen, C. Z. Huang and Y. F. Li, *Biosens. Bioelectron.*, 2021, **186**, 113263.
7 K. Shi, Z. Yang, L. Dong and B. Yu, *Sens. Actuators, B*, 2018, **266**, 263–269.
8 Y. Fan, D. Dong, Q. Li, H. Si, H. Pei, L. Li and B. Tang, *Lab Chip*, 2018, **18**, 1151–1173.
9 C. Lin, X. Song, W. Ye, T. Liu, M. Rong and L. Niu, *J. Anal. Test.*, 2023, DOI: **10.1007/s41664-023-00269-9**.
10 M. Wu, Z. W. Jiang, P. Zhang, X. Gong and Y. Wang, *Sens. Actuators, B*, 2023, **383**, 133596.
11 M. Rong, X. Yang, L. Huang, S. Chi, Y. Zhou, Y. Shen, B. Chen, X. Deng and Z. Q. Liu, *ACS Appl. Mater. Interfaces*, 2018, **11**, 2336–2343.
12 M. Rong, X. Deng, S. Chi, L. Huang, Y. Zhou, Y. Shen and X. Chen, *Microchim. Acta*, 2018, **185**, 1436–5073.
13 Y. Liu, M. Wang, Y. Hui, L. Sun, Y. Hao, H. Ren, H. Guo and W. Yang, *J. Mater. Chem. B*, 2024, **12**, 466–474.
14 J. Wu, P. Chen, J. Chen, X. Ye, S. Cao, C. Sun, Y. Jin, L. Zhang and S. Du, *Biosens. Bioelectron.*, 2022, **214**, 114538.
15 X. Wang, Y. Wang, X. Wang, C. Hu, X. Wu, W. Guo, S. Zhen, C. Huang and Y. Li, *Chem. Eng. J.*, 2022, **435**, 134912.
16 Z. Wu, M. Cai, W. Lv, C. Lu, B. Wu, C. Ren, Y. Dong, H. Chen and X. Chen, *Sens. Diagn.*, 2023, **2**, 1207–1214.
17 W. Y. Zhu, K. Liu and X. Zhang, *Sens. Diagn.*, 2023, **2**, 665–675.
18 R. Wang, H. Zhang, J. Sun and Z. Su, *Inorg. Chem. Front.*, 2024, **11**, 269–277.
19 C. Huang, R. Ma, Y. Luo, G. Shi, J. Deng and T. Zhou, *Anal. Chem.*, 2020, **92**, 12934–12942.
20 Y. Cao, Z. Wang, B. Fu, H. Li, X. Zhang, D.-Y. Guo, L. Li and Q. Pan, *Spectrochim. Acta, Part A*, 2023, **285**, 121915.
21 J. Wang, C. Jiang, J. Jin, L. Huang, W. Yu, B. Su and J. Hu, *Angew. Chem., Int. Ed.*, 2021, **60**, 13042–13049.
22 M. Naguib, M. Kurtoglu, V. Presser, J. Lu, J. Niu, M. Heon, L. Hultman, Y. Gogotsi and M. W. Barsoum, *Adv. Mater.*, 2011, **23**, 4248–4253.
23 Z. Guo, X. Zhu, S. Wang, C. Lei, Y. Huang, Z. Nie and S. Yao, *Nanoscale*, 2018, **10**, 19579–19585.
24 F. Wang, H. Wang, X. Cui and Y. Liu, *Sens. Diagn.*, 2022, **1**, 1080–1087.
25 M. Wang, S. Feng, C. Bai, K. Ji, J. Zhang, S. Wang, Y. Lu and D. Kong, *Small*, 2023, **19**, 2300386.
26 X. Tang, Y. Zhu, D. Duan, X. Zhai, Y. Xia, T. Xu, Q. Liu, H. Zhang and M. Zhou, *Adv. Funct. Mater.*, 2023, **33**, 2305965.
27 M. Song, Y. Ma, L. Li, M. C. Wong, P. Wang, J. Chen, H. Chen, F. Wang and J. Hao, *Mater. Des.*, 2022, **223**, 111249.
28 F. Ai, C. Fu, G. Cheng, H. Zhang, Y. Feng, X. Yan and X. Zheng, *ACS Appl. Nano Mater.*, 2021, **4**, 8192–8199, DOI: **10.1021/acsanm.1c01425**.
29 M. Liu, Y. He, J. Zhou, Y. Ge, J. Zhou and G. Song, *Anal. Chim. Acta*, 2020, **1103**, 134–142.
30 Q. Lu, J. Wang, B. Li, C. Weng, X. Li, W. Yang, X. Yan, J. Hong, W. Zhu and X. Zhou, *Anal. Chem.*, 2020, **92**, 7770–7777.
31 J. Yang, L. Chen, J. Qi, F. Luo, L. Li, H. Wu, F. Cao and J. Gu, *Food Chem.*, 2024, **430**, 137007.
32 T. Wang, W. Xiong, X. Tian and X. Xu, *Microchem. J.*, 2023, **194**, 109370.
33 J. Gu, X. Lu, G. Li, B. Shan, J. Liu, Y. Qu, H. Ye, K. Xi and H. Wu, *Chem. Eng. J.*, 2023, **467**, 143445.
34 X. Zheng, Z. Shi, C. Fu, Y. Ji, B. Chi, F. Ai and X. Yan, *Microchim. Acta*, 2023, **190**, 4.
35 D. Hu, S. Jiang, T. Xia, D. Xiao, Y. Li, Y. Hou, J. Z. Zhang and Y.-C. Pu, *Nano Res.*, 2023, DOI: **10.1007/s12274-023-6134-8**.
36 Q. Guan, J. Ma, W. Yang, R. Zhang, X. Zhang, X. Dong, Y. Fan, L. Cai, Y. Cao, Y. Zhang, N. Li and Q. Xu, *Nanoscale*, 2019, **11**, 14123–14133.
37 Y. Bai, Y. He, Y. Wang and G. Song, *Microchim. Acta*, 2021, **188**, 1436–5073.
38 X. Chen, X. Sun, W. Xu, G. Pan, D. Zhou, J. Zhu, H. Wang, X. Bai, B. Dong and H. Song, *Nanoscale*, 2018, **10**, 1111–1118.
39 Z. Wei, L. Yu, S. Wang, S. Li and Y. Xiao, *Sens. Actuators, B*, 2023, **377**, 133026.
40 D. Ren, X. Cheng, Q. Chen, G. Xu, F. Wei, J. Yang, J. Xu, L. Wang, Q. Hu and Y. Cen, *Microchem. J.*, 2023, **187**, 108397.
41 F. Yan, J. Sun, Y. Zang, Z. Sun, H. Zhang, J. Xu and X. Wang, *Dyes Pigm.*, 2021, **195**, 109720.
42 A. M. Al-Dhahebi, R. Jose, M. Mustapha and M. S. M. Saheed, *Food Chem.*, 2022, **390**, 133105.
43 S. Lu, L. Sui, Y. Liu, X. Yong, G. Xiao, K. Yuan, Z. Liu, B. Liu, B. Zou and B. Yang, *Adv. Sci.*, 2019, **6**, 1801470.
44 M. Rong, D. Wang, Y. Li, Y. Zhang, H. Huang, R. Liu and X. Deng, *J. Anal. Test.*, 2021, **5**, 51–59.
45 X. Zhou, J. Zhang, D. Huang, Y. Yi, K. Wu and G. Zhu, *Spectrochim. Acta, Part A*, 2023, **293**, 122484.

46 Q. Xue, H. Zhang, M. Zhu, Z. Pei, H. Li, Z. Wang, Y. Huang, Y. Huang, Q. Deng, J. Zhou, S. Du, Q. Huang and C. Zhi, *Adv. Mater.*, 2017, **29**, 1604847.
47 Y. Bai, Y. He, M. Wang and G. Song, *Sens. Actuators, B*, 2022, **357**, 131410.
48 Q. Wu, N. Li, Y. Wang, Y. Liu, Y. Xu, S. Wei, J. Wu, G. Jia, X. Fang, F. Chen and X. Cui, *Biosens. Bioelectron.*, 2019, **144**, 111697.
49 Q. Xu, L. Ding, Y. Wen, W. Yang, H. Zhou, X. Chen, J. Street, A. Zhou, W. J. Ong and N. Li, *J. Mater. Chem. C*, 2018, **6**, 6360–6369.
50 M. Rong, Y. Liang, D. Zhao, B. Chen, C. Pan, X. Deng, Y. Chen and J. He, *Sens. Actuators, B*, 2018, **265**, 498–505.
51 J. Chi, Y. Song and L. Feng, *Biosens. Bioelectron.*, 2023, **241**, 115666.
52 R. Han, J. Yu, Y. Wang, Y. Chen, X. Zhang, R. Zhang, J. Jing and X. Zhang, *Sens. Actuators, B*, 2024, **398**, 134455.
53 J. Wang, D. Li, Y. Qiu, X. Liu, L. Huang, H. Wen and J. Hu, *Talanta*, 2020, **220**, 121377.
54 Y. Huang, S. Chen, W. Huang, X. Zhuang, J. Zeng, M. Rong and L. Niu, *Food Chem.*, 2024, **432**, 137292.
55 J. Wang, Y. Feng, X. Zhao, Y. Tian and Y. Duan, *Biosens. Bioelectron.*, 2023, **238**, 115562.
56 M. Rong, Y. Huang, X. Zhuang, Y. Ma, H. Xie, Y. Wu and L. Niu, *Sens. Actuators, B*, 2023, **393**, 134204.
57 M. Xiao, Z. Liu, N. Xu, L. Jiang, M. Yang and C. Yi, *ACS Sens.*, 2020, **5**, 870–878.
58 L. Qin, J. Cao, D. Lin, S. Xu, Y. Li and C. Jiang, *Chem. Eng. J.*, 2023, **464**, 142550.